Supplementary Information

Coexistence of superconductivity and electride states in Ca_2H with an antifluorite-type motif under compression

Qianyi Wang,[1] Shoutao Zhang,[1,*] Honggang Li,[1] Hongbo Wang,[2] Guangtao Liu,[2] Jiangang Ma,[1] Haiyang Xu,[1] Hanyu Liu,[2,*] and Yanming Ma[2]

[1]*Key Laboratory of UV-Emitting Materials and Technology of Ministry of Education, School of Physics, Northeast Normal University, Changchun 130024, China*

[2]*Key Laboratory of Material Simulation Methods and Software of Ministry of Education & State Key Laboratory of Superhard Materials, College of Physics, Jilin University, Changchun 130012, China*

[*]Corresponding Author Email: zhangst966@nenu.edu.cn; hanyuliu@jlu.edu.cn

Index **Page**

Computational Details

Our structural prediction approach is based on a global minimization of free energy surfaces merging *ab initio* total-energy calculations with CALYPSO (Crystal structure AnaLYsis by Particle Swarm Optimization) methodology as implemented in the CALYPSO code.[1,2] The structures of stoichiometry Ca_mH_n (m = 1-6, n = 1-2; m = 4, n = 3) were searched with simulation cell sizes up to 4 formula units (f.u.) at 0 K and the considered pressures of 20, 50, 100, 200, and 300 GPa. In the first step, random structures with certain symmetry are constructed in which atomic coordinates are generated by the crystallographic symmetry operations. Local optimizations using the VASP code[3] were done with the conjugate gradients method and stopped when Gibbs free energy changes became smaller than 1×10^{-5} eV per cell. After processing the first-generation structures, 60% of them with lower Gibbs free energies are selected to construct the next generation structures by PSO (Particle Swarm Optimization). 40% of the structures in the new generation are randomly generated. A structure fingerprinting technique of bond characterization matrix is applied to the generated structures, so that identical structures are strictly forbidden. These procedures significantly enhance the diversity of the structures, which is crucial for structural global search efficiency. In most cases, structural searching simulations for each calculation were stopped after generating 1000 ~ 1200 structures (e.g., about 20 ~ 30 generations).

To further analyze the structures with higher accuracy, we select a number of structures with lower total energies and perform structural optimization using density functional theory within the generalized gradient approximation (GGA)[4] as implemented in the VASP code. The cut-off energy for the expansion of wavefunctions into plane waves is set to 800 eV in all calculations, and the Monkhorst–Pack k-mesh with a maximum spacing of $2\pi \times 0.03$ Å^{-1} was individually adjusted in reciprocal space with respect to the size of each computational cell. This usually gives total energies well converged within ~1 meV/atom. The electron-ion interaction was described by using all-electron projector augmented-wave (PAW) method with $3s^2 3p^6 4s^2$ and $1s^1$ valence electrons for Ca and H atoms, respectively. The formation enthalpy (ΔH_f) relative to the elemental solids (Ca[5–8] and CaH_2[9,10]), was calculated at each considered pressure according to the equation below:

$$\Delta H_f(Ca_mH_n) = [H(Ca_mH_n) - (m-\frac{n}{2})H(Ca) - \frac{n}{2}H(CaH_2)]/(m+n), \qquad (1)$$

where ΔH_f is the formation energy per atom of the given compound. $H(Ca_mH_n)$, $H(Ca)$, and $H(CaH_2)$ are enthalpies of each Ca_mH_n composition, elemental Ca, and CaH_2, respectively.

To determine the dynamical stability of predicted structures, phonon calculations were performed by using the finite displacement approach[11] as implemented in the Phonopy code.[12]

The electron-phonon coupling calculations are carried out with the density functional perturbation (linear

response) theory as implemented in the QUANTUM ESPRESSO package.[13] We employ the ultrasoft pseudopotentials with $3s^2 3p^6 4s^2$ and $1s^1$ as valence electrons of Ca and H atoms, respectively. The kinetic energy cutoff for wave-function expansion is chosen as 80 Ry. To reliably calculate electron-phonon coupling (EPC) in metallic systems, we need to sample dense *k*-meshes for the electronic Brillouin zone integration and enough *q*-meshes for evaluating average contributions from the phonon modes. Dependent *k*-meshes and *q*-meshes on *Fm*-3*m* Ca_2H as well as *Fm*-3*m* A_2H (A = Li, Na, K, and Rb) are used, namely, 8 × 8 × 8 *k*-meshes and 4 × 4 × 4 *q*-meshes. We have calculated the superconducting T_c as estimated from the McMillan formula:[14,15]

$$T_c = \frac{\omega_{log}}{1.2} exp\left\{ -\frac{1.04(1+\lambda)}{\lambda - \mu^*(1+0.62\lambda)} \right\}, \quad (2)$$

Here, ω_{log} is the logarithmic average phonon frequency, and μ^* is the Coulomb pseudopotential with a typical value of 0.1. Additionally, the Allen-Dynes modified McMillan equation[16] with factors f_1 and f_2 is exploited, when λ is greater than 1.5. The factors f_1 and f_2 depend on $\lambda, \mu^*, \omega_{log}$, and $\bar{\omega}_2$ (mean square frequency).

$$T_c = f_1 f_2 \frac{\omega_{log}}{1.2} exp\left[-\frac{1.04(1+\lambda)}{\lambda - \mu^*(1+0.62\lambda)} \right], \quad (3)$$

$$f_1 = \left[1 + \left(\frac{\lambda}{2.46(1+3.8\mu^*)} \right)^{\frac{3}{2}} \right]^{\frac{1}{3}} \quad (4)$$

$$f_2 = 1 + \frac{\left(\frac{\bar{\omega}_2}{\omega_{log}} - 1 \right)\lambda^2}{\lambda^2 + \left[1.82(1+6.3\mu^*)\frac{\bar{\omega}_2}{\omega_{log}} \right]^2} \quad (5)$$

$$\bar{\omega}_2 = \langle \omega^2 \rangle^{\frac{1}{2}} \quad (6)$$

The frequency-dependent EPC parameter $\lambda(\omega)$ is calculated by Eliashberg spectral function $\alpha^2F(\omega)$,

$$\lambda(\omega) = 2\int_0^\infty \frac{\alpha^2 F(\omega)}{\omega} d\omega, \quad (7)$$

with total EPC parameter λ shown in the T_c equation, and

$$\alpha^2 F(\omega) = \frac{1}{2}\sum_j \int_{BZ} \frac{dq}{\Omega_{BZ}} \omega_{qj}\lambda_{qj}\delta(\omega - \omega_{qj})$$

Herein, the integration is over the first Brillouin zone (BZ), with Ω_{BZ} as the volume of the BZ. The $\boldsymbol{q}$ denotes

the phonon wave vector. The phonon frequency of mode j at wave vector $\boldsymbol{q}$ is represented by $\omega_{\boldsymbol{q}j}$. The frequency-dependent EPC parameter for mode j at wave vector $\boldsymbol{q}$ is $\lambda_{qj} = \gamma_{qj}/\pi\hbar N_F \omega_{qj}^2$, where the linewidth for mode j at wave vector $\boldsymbol{q}$ is

$$\gamma_{qj} = 2\pi\omega_{qj}\sum_{nm}\int_{BZ}\left[(dk)/(\Omega_{BZ})\right]\left|g_{kn,k+qm}^{j}\right|^2\delta(\varepsilon_{kn}-\varepsilon_F)\delta(\varepsilon_{k+qm}-\varepsilon_F)$$

.

N_F is the electronic density of states at the Fermi level. ε_{kn} is the energies of bands with respect to the Fermi level ε_F at $\boldsymbol{k}$. Here, $g_{kn,k+qm}^{j}$ is the electron-phonon matrix element for the scattering of an electron in band n at wave vector $\boldsymbol{k}$ state to band m at wave vector $\boldsymbol{k}$+$\boldsymbol{q}$ state via a phonon with wave vector $\boldsymbol{q}$.

Supporting Figures

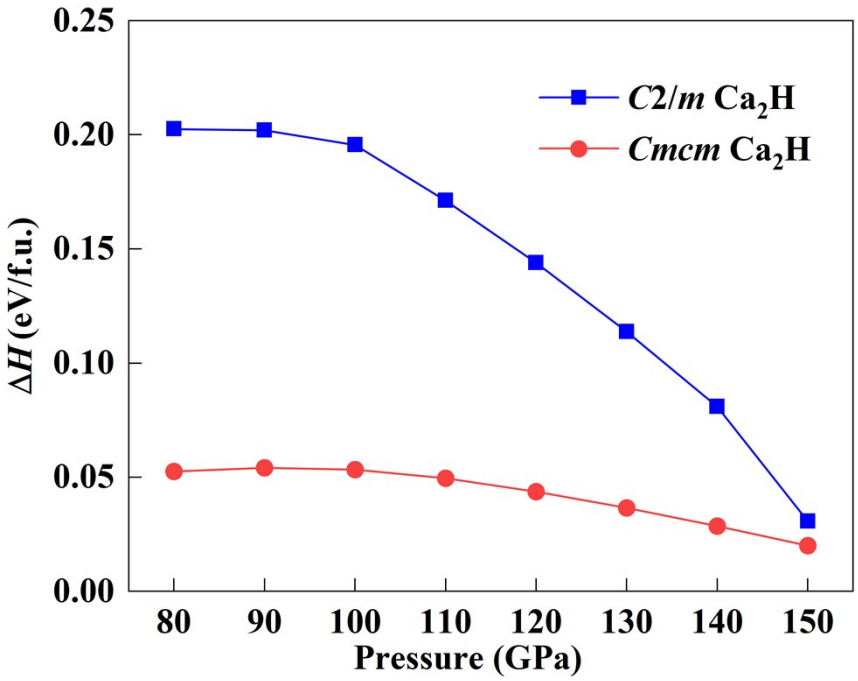

Figure S1. Calculated ΔH as a function of pressure of reported Ca_2H with respect to *Fm*-3*m* Ca_2H. The enthalpy difference (ΔH) is defined as $\Delta H = H(C2/m\ Ca_2H) - H(Fm\text{-}3m\ Ca_2H)$ (blue line); $\Delta H = H(Cmcm\ Ca_2H) - H(Fm\text{-}3m\ Ca_2H)$ (red line).

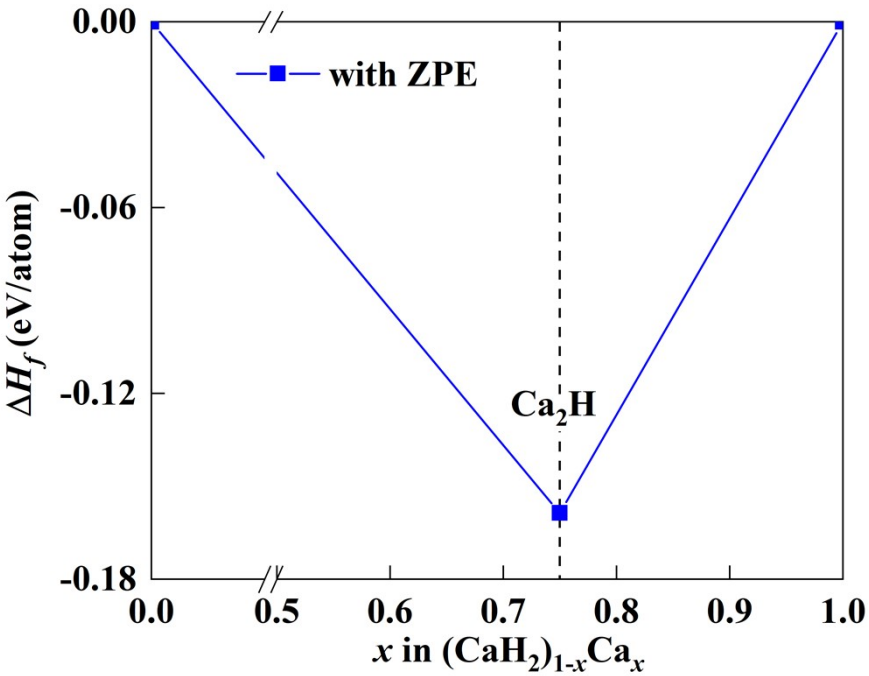

Figure S2. The convex hull diagram with zero-point energy (ZPE) of *Fm*-3*m* Ca_2H at 100 GPa.

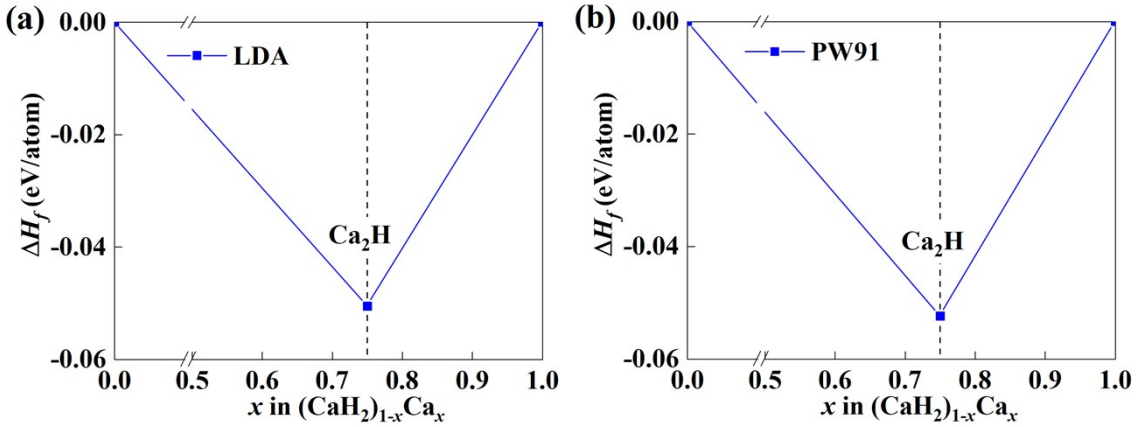

Figure S3. The convex hull diagram with (a) local density approximation (LDA)[17] and (b) Perdew-Wang 91 (PW91)[18] functionals of *Fm*-3*m* Ca_2H at 100 GPa.

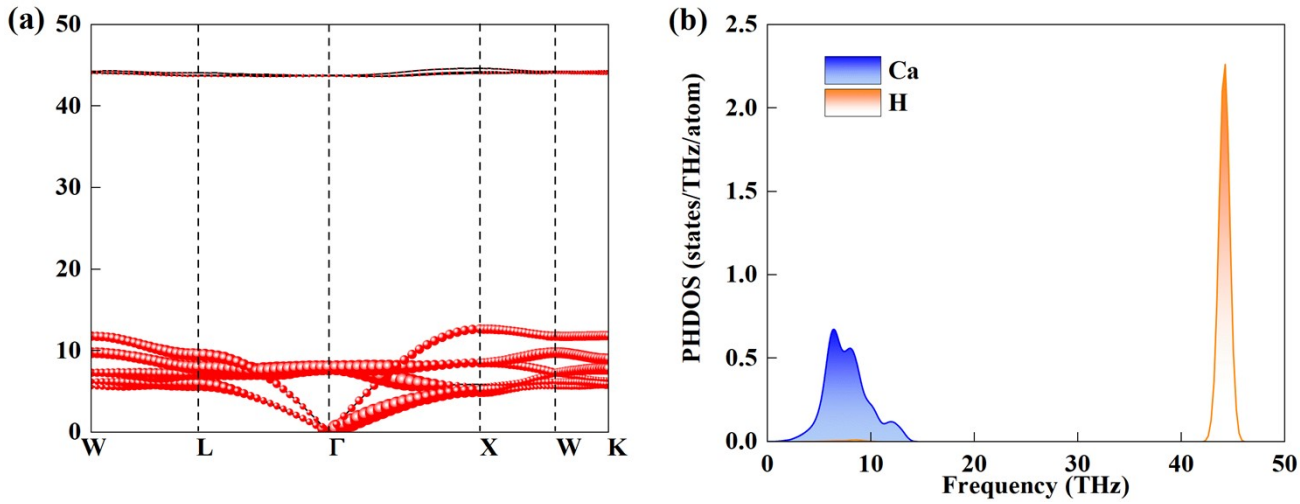

Figure S4. (a) Phonon spectrum with the size of red ball denoting the contribution to electron-phonon coupling of *Fm*-3*m* Ca_2H at 100 GPa (b) Phonon density of states (PHDOS) of *Fm*-3*m* Ca_2H at 100 GPa.

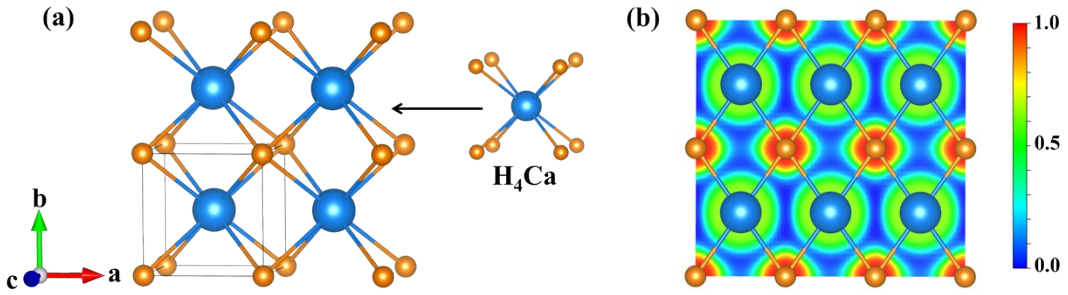

Figure S5. Electron localization function (ELF) of *Pm*-3*m* CaH at 200 GPa. The ELF analysis can be used to distinguish different types of chemical bonds. Generally, covalent bonds, lone electron pairs, and core electrons are represented by large values (> 0.5), whereas small values (< 0.5) correspond to ionic bonds. The ELF value of 0.5 denotes metallic bonding.

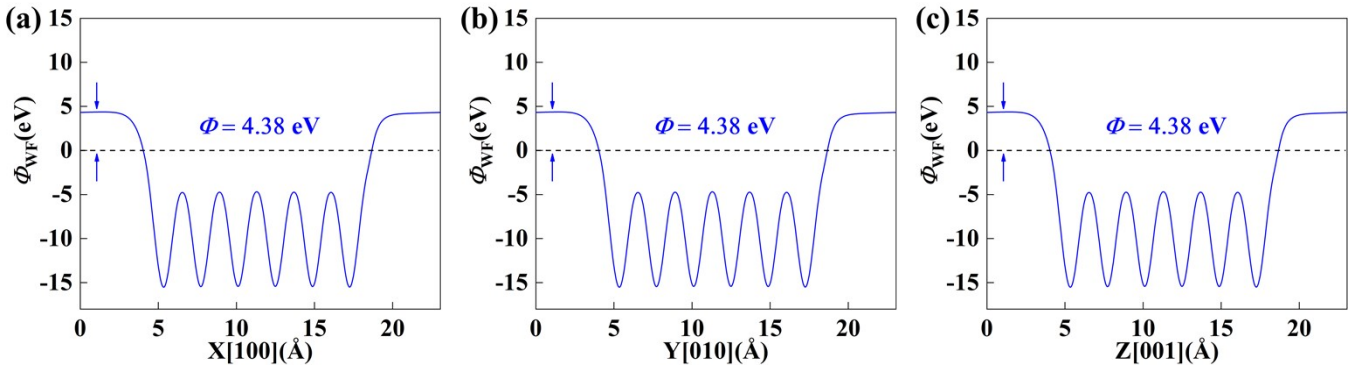

Figure S6. Calculated work function of *Fm*-3*m* Ca_2H at 100 GPa along [100], [010], and [001] directions.

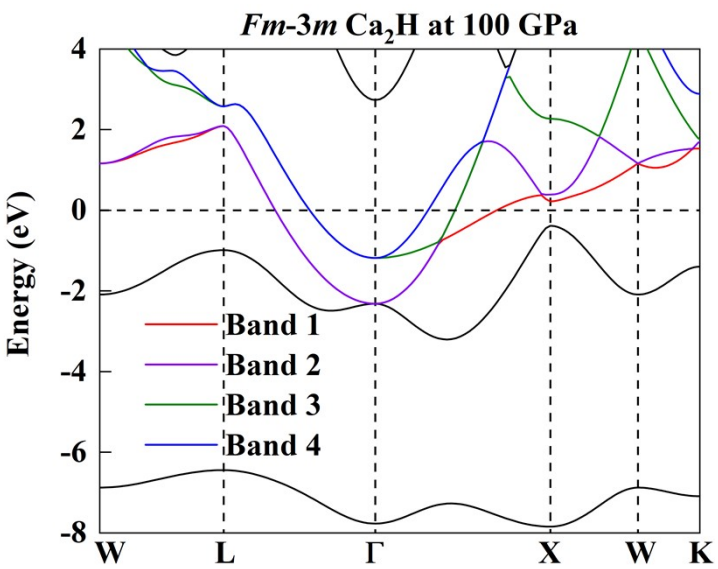

Figure S7. Electronic band structure of *Fm*-3*m* Ca_2H at 100 GPa wherein there are four bands crossing the Fermi level E_F.

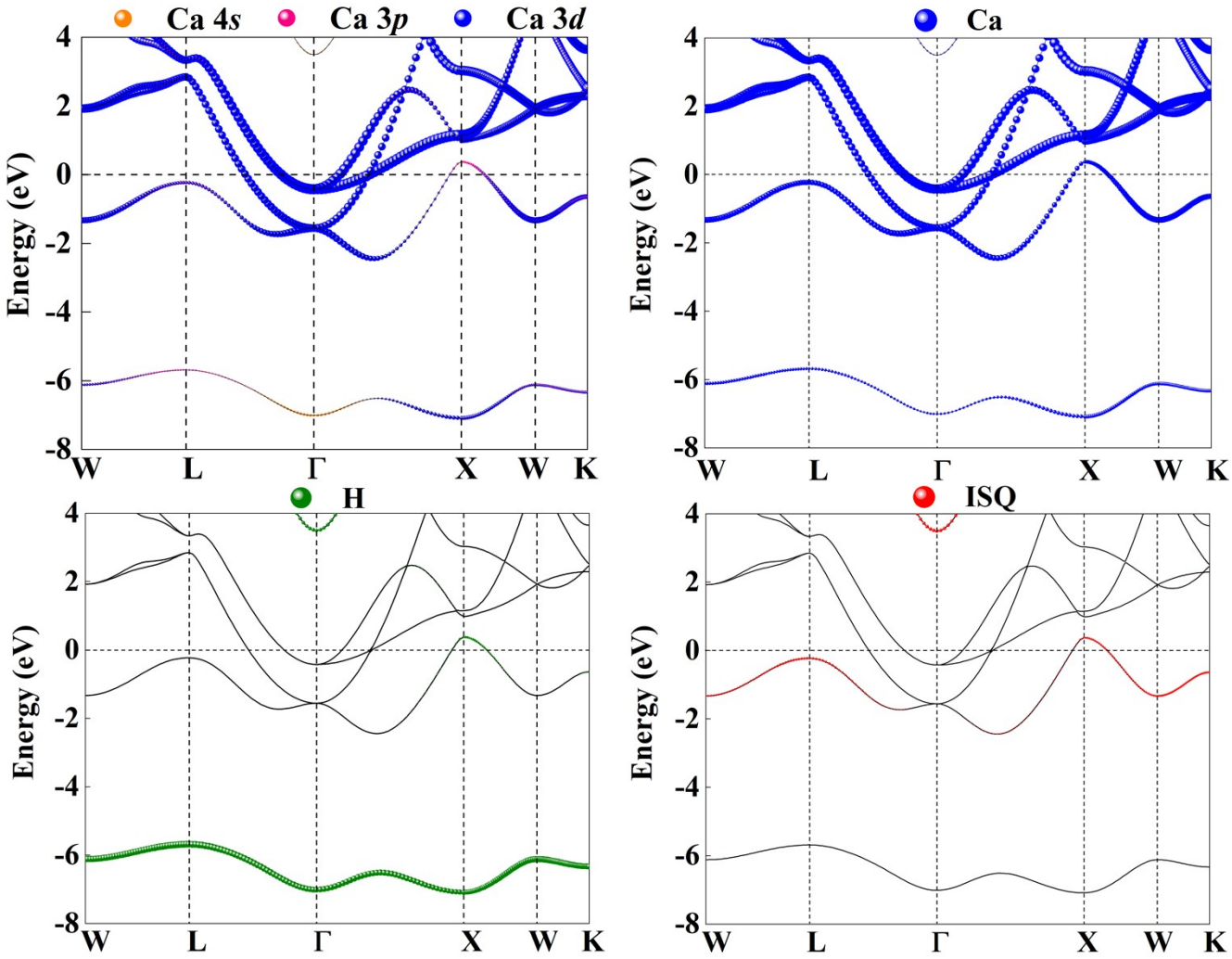

Figure S8. Orbital projected electronic band structure of *Fm*-3*m* Ca_2H at 100 GPa. The contribution of Ca, H and ISQ atomic orbitals (Ca 3*s*, Ca 3*p*, Ca 3*d*, H, and ISQ) is illustrated by the size of the solid circles.

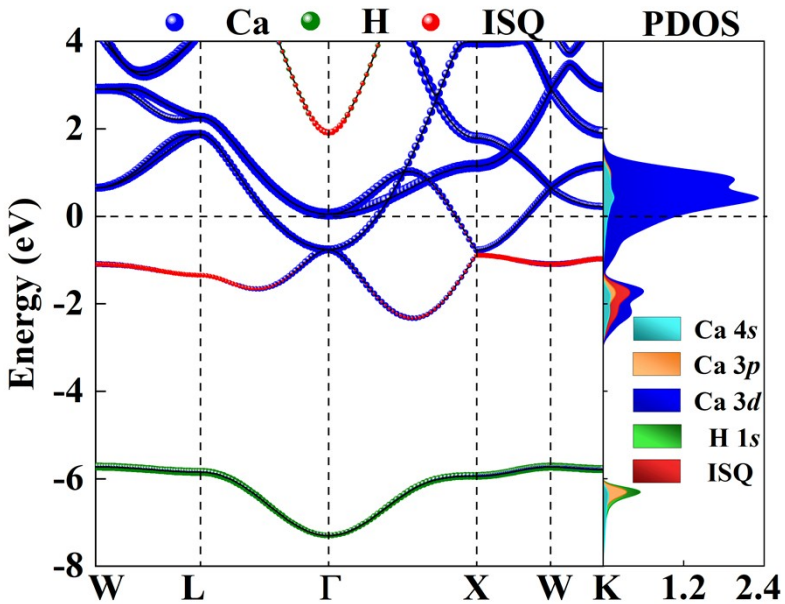

Figure S9. Orbital-projected electronic band structure and projected density of states (PDOS) (states/eV/f.u.) of *Fm*-3*m* Ca_2H at 30 GPa. The size of the circles represents the magnitude of contribution of Ca, H, and ISQ. The Fermi level is denoted by the horizontal dashed line.

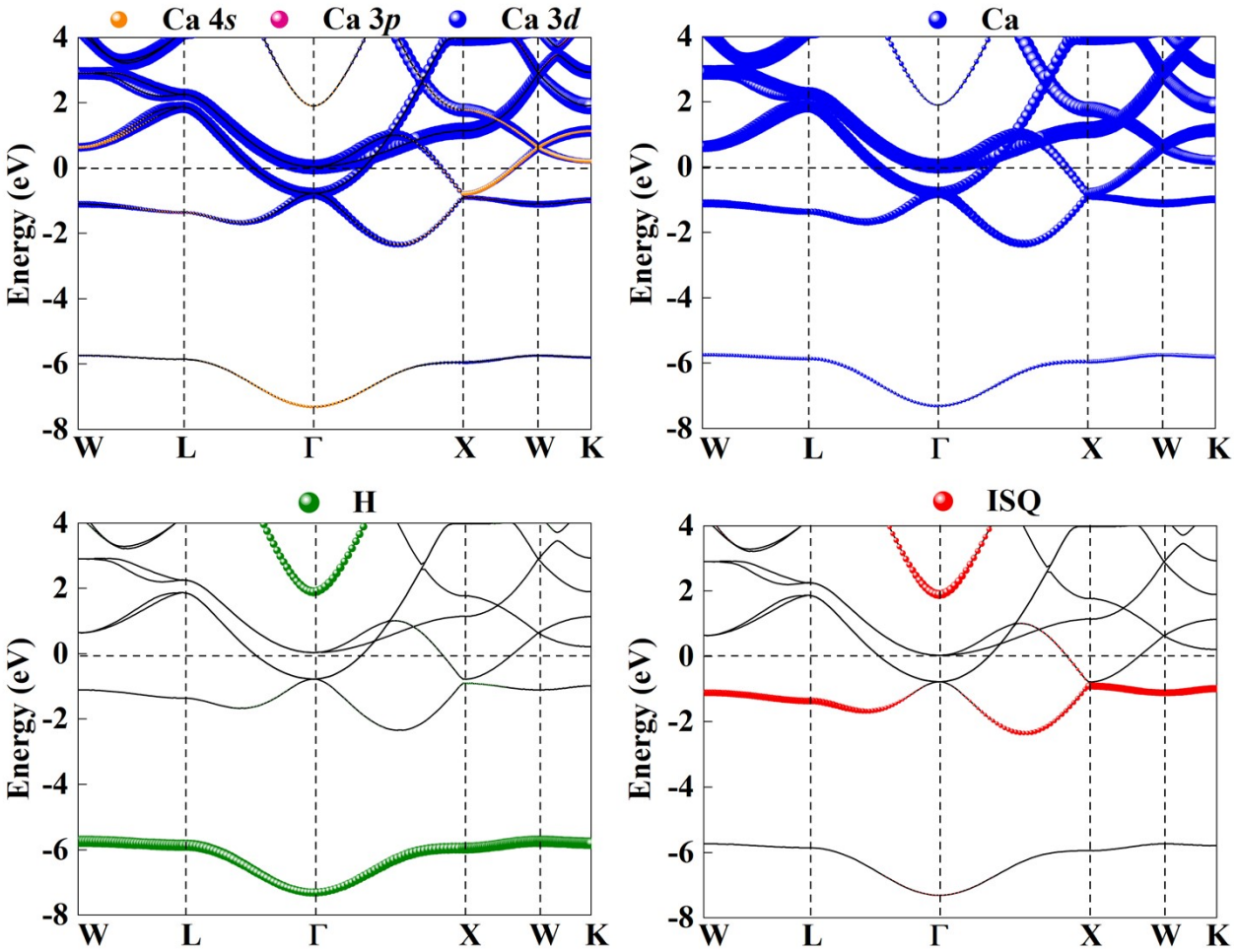

Figure S10. Orbital projected electronic band structure of *Fm*-3*m* Ca_2H at 30 GPa. The contribution of Ca, H and ISQ atomic orbitals (Ca 3*s*, Ca 3*p*, Ca 3*d*, H, and ISQ) is illustrated by the size of the solid circles.

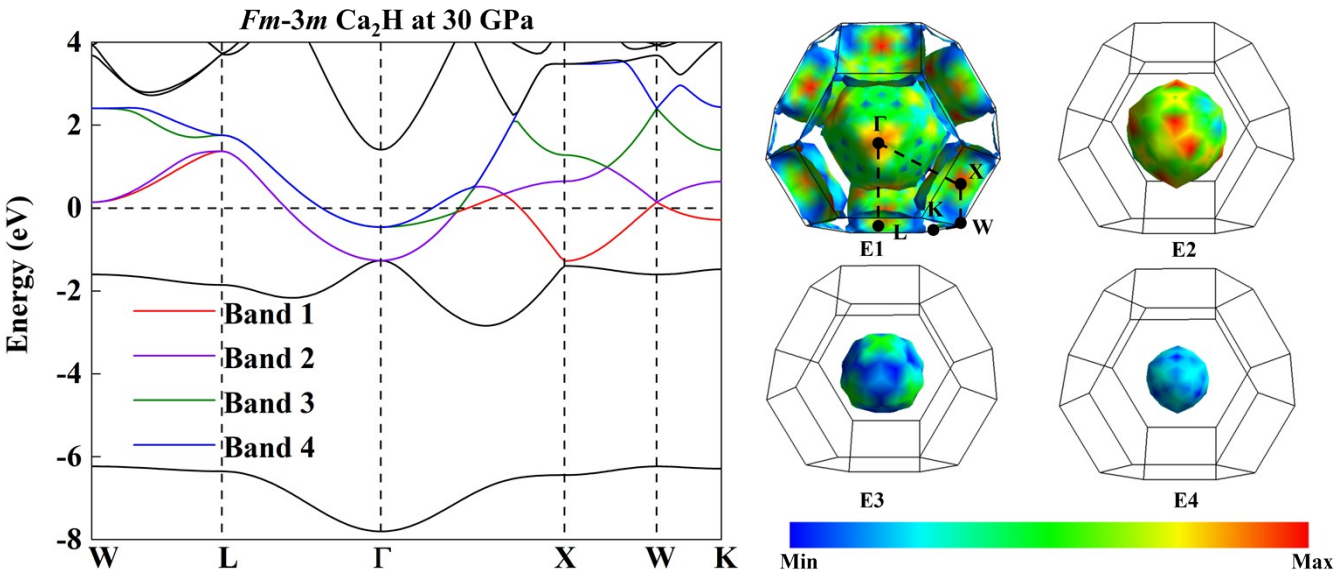

Figure S11. Fermi surfaces corresponding to the four bands crossing the E_F and color coded by the Fermi velocity of *Fm*-3*m* Ca_2H at 30 GPa.

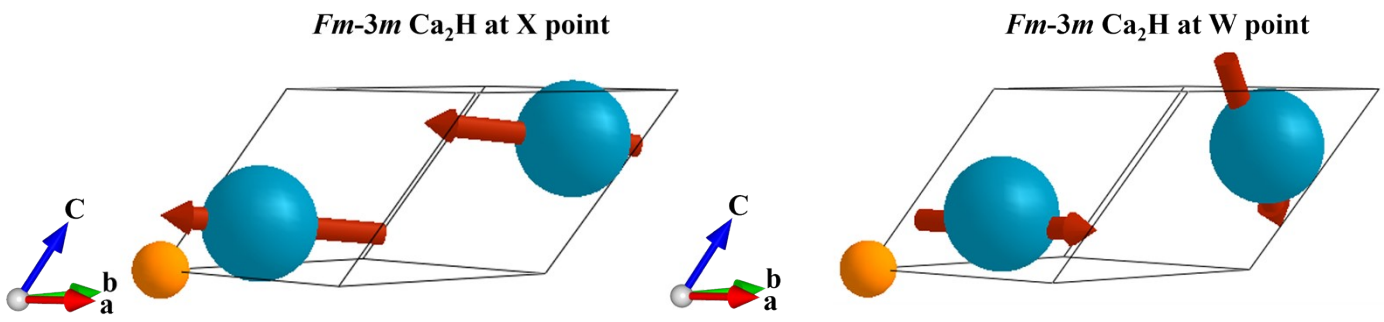

Figure S12. The vibrational modes with the lowest-frequency acoustic branch at X and W points for *Fm*-3*m* Ca_2H at 30 GPa are indicated by arrows. The blue and orange balls represent calcium and hydrogen atoms, respectively.

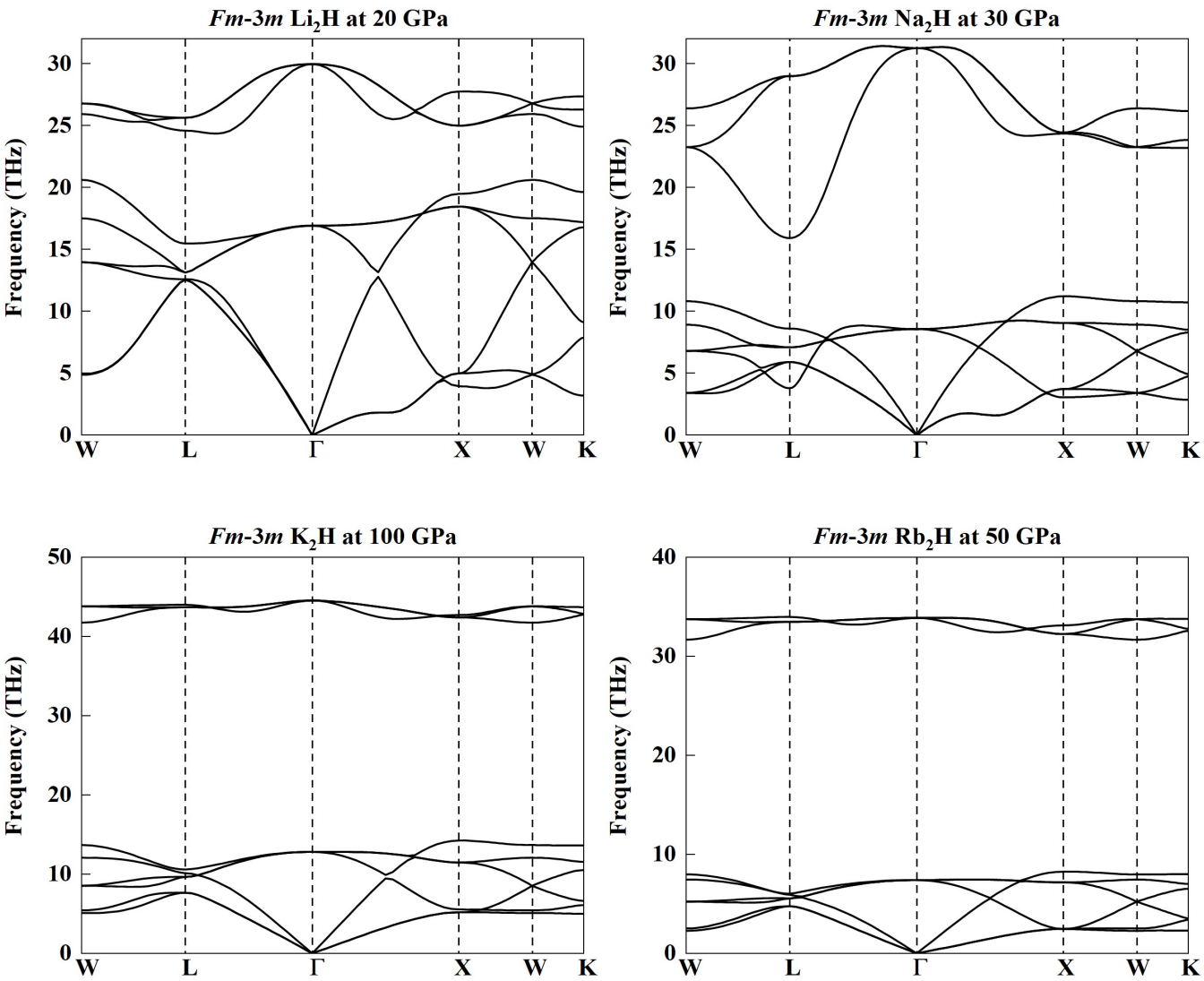

Figure S13. Phonon dispersion curves of *Fm*-3*m* A_2H (A = Li, Na, K, and Rb) at pressures. The results show that *Fm*-3*m* A_2H (A = Li, Na, K, and Rb) are dynamically stable.

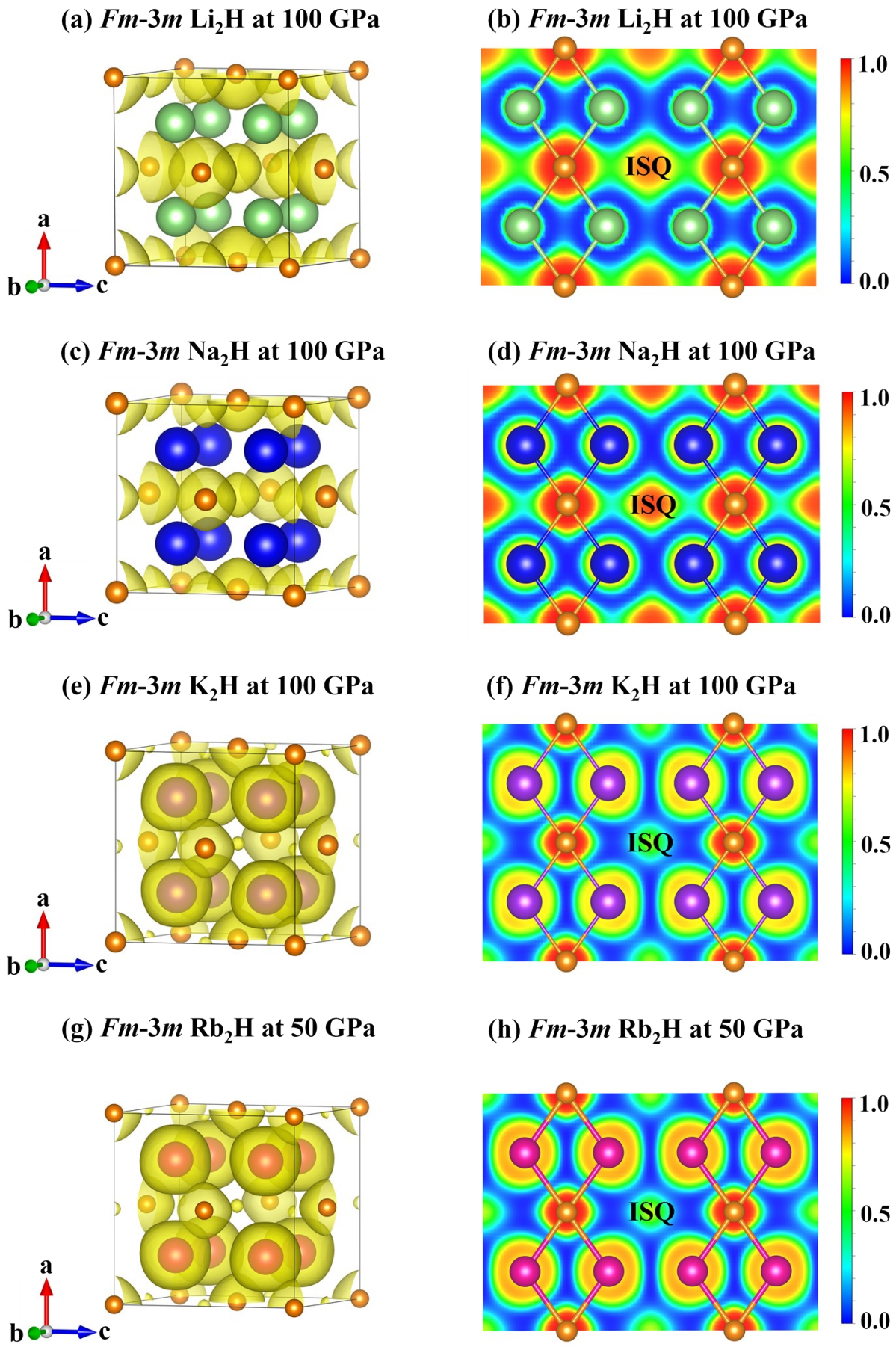

Figure S14. Electron localization function (ELF) of *Fm*-3*m* A_2H (A = Li, Na, K, and Rb). The results suggest that zero-dimensional (0D) electron distribution is revealed in Li_2H, Na_2H, K_2H, and Rb_2H.

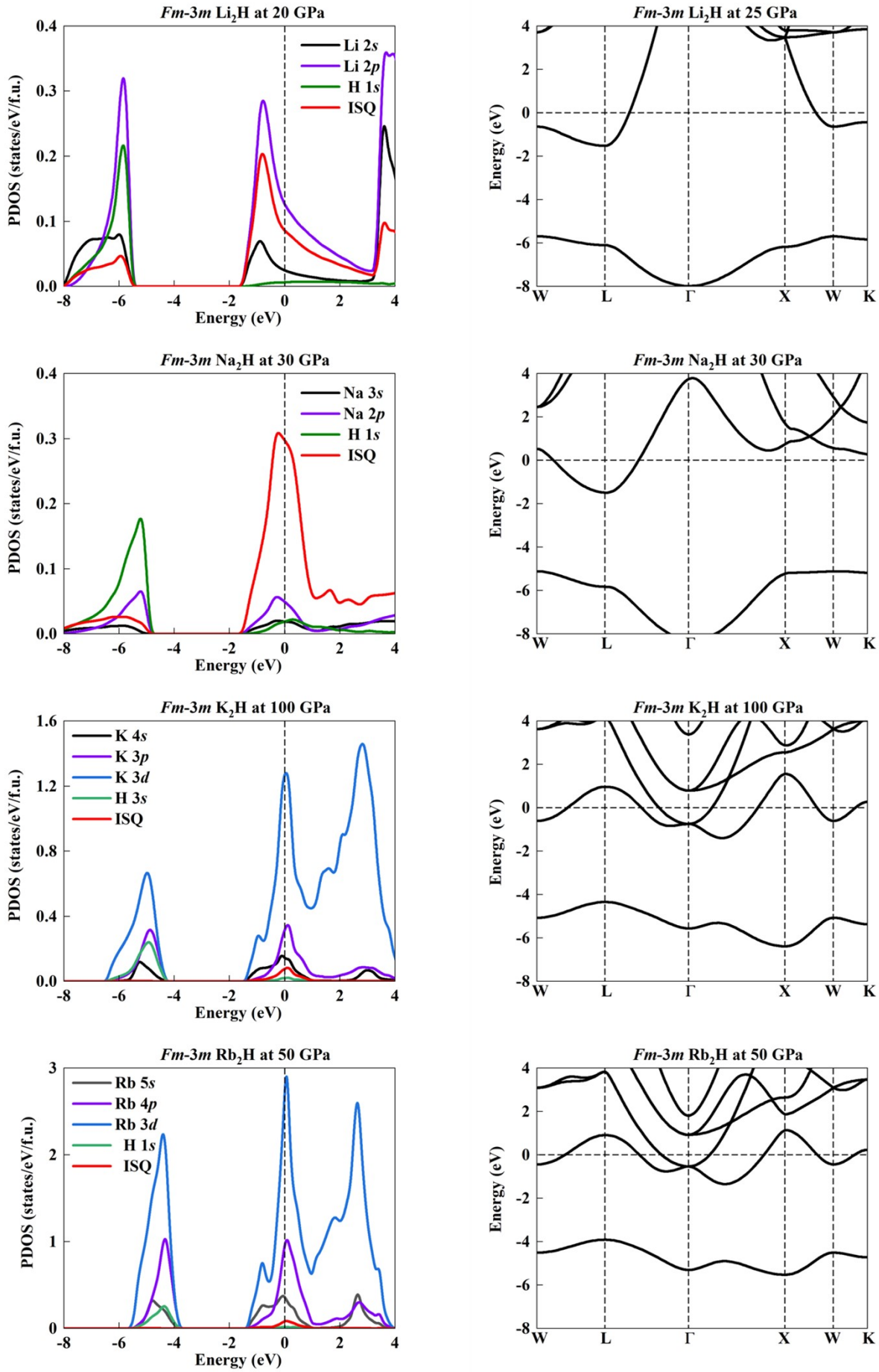

Figure S15. Electronic band structures and projected density of states (PDOS) of *Fm*-3*m* A_2H (A = Li, Na, K, and Rb) at different pressures.

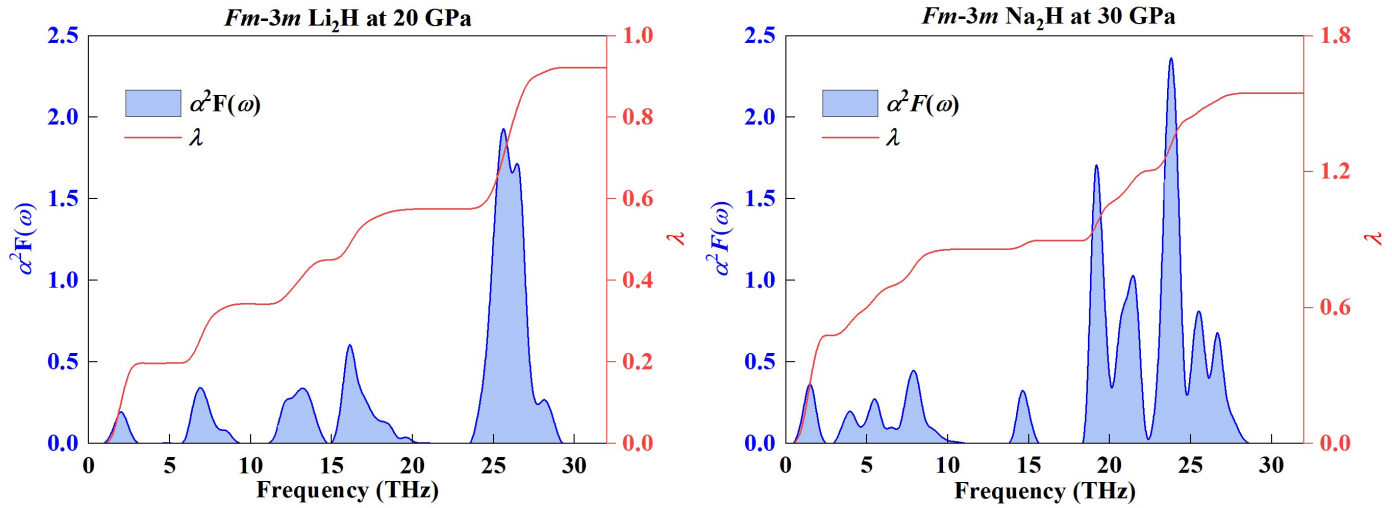

Figure S16. Eliashberg spectral function $\alpha^2F(\omega)$ (blue area), EPC parameter $\lambda(\omega)$ (red line), and Phonon density of states (PHDOS) as a function of frequency ω of *Fm*-3*m* Li_2H at 20 GPa and *Fm*-3*m* Na_2H at 30 GPa.

Supporting Tables

Table S1. Structural information of the predicted Ca_2H.

Phase	Pressure (GPa)	Lattice Parameters (Å,°)	Atoms	Wyckoff Positions (fractional)		
				x	*y*	*z*
***Fm*-3*m* Ca_2H**	100	a = 4.76878	Ca (8c)	0.7500	0.2500	0.7500
		b = 4.76878	H (4a)	0.0000	0.0000	0.0000
		c = 4.76878				
		α =90.0000				
		β =90.0000				
		γ =90.0000				

Table S2. Calculated Bader atomic charge of the *Fm*-3*m* Ca_2H at different pressures by the Bader charge analysis[19].

Phases	Pressure (GPa)	Atoms	Charge (e)
***Fm*-3*m* Ca_2H**	30	Ca	0.670
		H	-0.857
		ISQ	-0.483
***Fm*-3*m* Ca_2H**	50	Ca	0.620
		H	-0.810
		ISQ	-0.430
***Fm*-3*m* Ca_2H**	100	Ca	0.486
		H	-0.672
		ISQ	-0.300

Table S3. Laplacian of charge density $\nabla^2\rho(r)$ and charge density $\rho(r)$ of *Fm*-3*m* Ca_2H at 100 GPa.

Phases	Pressure (GPa)	Selected Atoms	$\nabla^2\rho$ (e/Å^5)	$\rho(r)$ (e/Å^3)
***Fm*-3*m* Ca_2H**	100 GPa	Ca-H	0.26176	0.0406
		Ca-Ca	0.13883	0.0478
		Ca-ISQ	0.00051	0.0325

Table S4. Bader atomic charge of *Fm*-3*m* A_2H (A = Li, Na, K, and Rb).

Phases	Pressure (GPa)	Atoms	Charge (e)
***Fm*-3*m* Li_2H**	20	Li	0.772
		H	-1.240
		ISQ	-0.304
***Fm*-3*m* Na_2H**	30	Na	0.640
		H	-0.843
		ISQ	-0.437
***Fm*-3*m* K_2H**	100	K	0.310
		H	-0.575
		ISQ	-0.045
***Fm*-3*m* Rb_2H**	50	Rb	0.343
		H	-0.637
		ISQ	-0.049

Table S5. Superconducting properties of *Fm*-3*m* Ca_2H and A_2H (A = Li, Na, K, and Rb).

Phases	**Pressure**	λ	ω_{log} **(K)**	$N(E_f)$ **(states/Ry/cell)**	T_c **(K)**	$f_1f_2T_c$ **(K)**
***Fm*-3*m* Ca_2H**	100 GPa	0.56	337.1	7.4	6.1	
***Fm*-3*m* Ca_2H**	50 GPa	0.73	251.7	10.9	9.6	
***Fm*-3*m* Ca_2H**	30 GPa	1.01	155.5	13.1	11.1	
***Pm*-3*m* CaH**	200 GPa	0.52	618.1	4.4	8.9	
***Pm*-3*m* CaH**	100 GPa	0.84	416.9	6.7	21.5	
***Pm*-3*m* CaH**	50 GPa	1.81	184.1	8.8	24.7	29.9
***Fm*-3*m* Li_2H**	100 GPa	0.54	1116.1	2.4	18.7	
***Fm*-3*m* Li_2H**	50 GPa	0.58	970.1	2.8	20.4	
***Fm*-3*m* Li_2H**	30 GPa	0.74	657.8	3.2	25.9	
***Fm*-3*m* Li_2H**	20 GPa	0.92	532.1	3.4	32.5	
***Fm*-3*m* Na_2H**	100 GPa	0.52	779.8	7.0	10.9	
***Fm*-3*m* Na_2H**	50 GPa	0.81	601.2	6.9	29.2	
***Fm*-3*m* Na_2H**	30 GPa	1.53	338.9	7.0	39.4	45.7
***Fm*-3*m* K_2H**	100 GPa	0.35	532.0	10.2	0.9	
***Fm*-3*m* Rb_2H**	100 GPa	0.6	324.0	9.2	7.4	
***Fm*-3*m* Rb_2H**	50 GPa	0.32	347.3	10.4	0.3	

References

1 Y. Wang, J. Lv, L. Zhu and Y. Ma, *Phys. Rev. B*, 2010, **82**, 094116.

2 Y. Wang, J. Lv, L. Zhu and Y. Ma, *Comput. Phys. Commun.*, 2012, **183**, 2063–2070.

3 G. Kresse and J. Furthmüller, *Phys. Rev. B*, 1996, **54**, 11169–11186.

4 J. P. Perdew, J. A. Chevary, S. H. Vosko, K. A. Jackson, M. R. Pederson, D. J. Singh and C. Fiolhais, *Phys. Rev. B*, 1993, **48**, 4978.

5 T. Yabuuchi, Y. Nakamoto, K. Shimizu and T. Kikegawa, *J. Phys. Soc. Japan*, 2013, **74**, 2391–2392.

6 H. Fujihisa, Y. Nakamoto, K. Shimizu, T. Yabuuchi and Y. Gotoh, *Phys. Rev. Lett.*, 2008, **101**, 095503.

7 Y. Nakamoto, M. Sakata, K. Shimizu, H. Fujihisa, T. Matsuoka, Y. Ohishi and T. Kikegawa, *Phys. Rev. B*, 2010, **81**, 140106.

8 A. R. Oganov, Y. Ma, Y. Xu, I. Errea, A. Bergara and A. O. Lyakhov, *Proc. Natl. Acad. Sci. U. S. A.*, 2010, **107**, 7646–7651.

9 Y. Li, B. Li, T. Cui, Y. Li, L. Zhang, Y. Ma and G. Zou, *J. Phys. Condens. Matter*, 2008, **20**, 045211.

10 J. S. Tse, D. D. Klug, S. Desgreniers, J. S. Smith, R. Flacau, Z. Liu, J. Hu, N. Chen and D. T. Jiang, *Phys. Rev. B*, 2007, **75**, 134108.

11 K. Parlinski, Z. Q. Li and Y. Kawazoe, *Phys. Rev. Lett.*, 1997, **78**, 4063–4066.

12 A. Togo, F. Oba and I. Tanaka, *Phys. Rev. B*, 2008, **78**, 134106.

13 P. Giannozzi, S. Baroni, N. Bonini, M. Calandra, R. Car, C. Cavazzoni, D. Ceresoli, G. L. Chiarotti, M. Cococcioni and I. Dabo, *J. Phys. Condens. matter*, 2009, **21**, 395502.

14 W. L. McMillan, *Phys. Rev.*, 1968, **167**, 331.

15 R. C. Dynes, *Solid State Commun.*, 1972, **10**, 615–618.

16 P. B. Allen and R. C. Dynes, *Phys. Rev. B*, 1975, **12**, 905–922.

17 D. M. Ceperley and B. J. Alder, *Phys. Rev. Lett.*, 1980, **45**, 566–569.

18 J. P. Perdew, J. A. Chevary, S. H. Vosko, K. A. Jackson, M. R. Pederson, D. J. Singh and C. Fiolhais, *Phys. Rev. B*, 1992, **46**, 6671–6687.

19 R. F. W. Bader, *Acc. Chem. Res.*, 1985, **18**, 9–15.